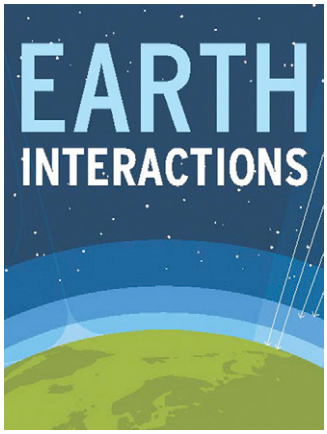


Copyright © 2015, Paper 19-015; 57201 words, 12 Figures, 0 Animations, 3 Tables.
http://EarthInteractions.org

Changes in Tropical Cyclone Activity over Northwest Western Australia in the Past 50 Years and a View of the Future 50 Years

Diandong Ren*

Department of Imaging and Applied Physics, Curtin University, and Australian Sustainable Development Institute, Curtin University, Perth, Western Australia, Australia

Lance M. Leslie

School of Meteorology, University of Oklahoma, Norman, Oklahoma

Received 13 September 2013; in final form 20 May 2015

ABSTRACT: In the first half of this research, this study examines the trend in tropical cyclone (TC) activity over the economically important northwest Western Australia (NWA) TC basin (equator–40°S, 80°–140°E) based on statistical analyses of the International Best Track Archive for Climate Stewardship (IBTrACS) and large-scale environmental variables, which are known to be closely linked to the formation and longevity of TCs, from NCEP–NCAR reanalyses. In the second half, changes in TC activity from climate model

* Corresponding author address: Dr. Diandong Ren, Department of Physics, Curtin University of Technology, GPO Box U1987, Perth, WA 6845.
E-mail address: rendianyun@gmail.com

DOI: 10.1175/EI-D-14-0006.1

projections for 2000–60 are compared for (i) no scenario change (CNTRL) and (ii) the moderate IPCC Special Report on Emission Scenarios (SRES) A1B scenario (EGHG). The aims are to (i) determine differences in mean annual TC frequency and intensity trends, (ii) test for differences between genesis and decay positions of CNTRL and EGHG projections using a nonparametric permutation test, and (iii) use kernel density estimation (KDE) for a cluster analysis of CNTRL and EGHG genesis and decay positions and generate their probability distribution functions.

The main findings are there is little difference in the mean TC number over the period, but there is a difference in mean intensity; CNTRL and EGHG projections differ in mean genesis and decay positions in both latitude and longitude; and the KDE reveals just one cluster in both CNTRL and EGHG mean genesis and decay positions. The EGHG KDE is possibly disjoint, with a wider longitudinal spread. The results can be explained in terms of physical, meteorological, and sea surface temperature (SST) conditions, which provide natural limits to the spread of the genesis and decay points.

KEYWORDS: Geographic location/entity; Australia

1. Introduction

Tropical cyclones (TCs) are the most devastating weather systems (Henderson-Sellers et al. 1998) that affect resource-rich northwest Western Australia (NWA; equator–40°S, 80°–140°E; Figure 1), as they often generate strong winds, large waves and swell, and severe flooding from both heavy rainfall and high storm surges. The NWA basin is relatively less well studied because of its historically low population density. However, the economic and societal costs of TCs are very high as they affect both land-based and offshore structures by disrupting mining operations, closing and damaging seaports, and necessitating the shutdown and evacuation of oil and natural gas facilities. For example, in the Pilbara and Kimberley regions of NWA, there are particularly large investments in offshore infrastructure associated with the production of liquid petroleum and natural gas (approximately AUD $25 billion value each year). The economic consequences of tropical cyclones in the northwest (NW) region of Australia are significant. The offshore oil and gas infrastructure, the numerous coastal port facilities, and the onshore iron ore mining infrastructure investment in the adjacent Pilbara region are substantial (approximately AUD $56 billion in 2012–13). The region consequently is a major contributor to the value of Western Australia's mineral and petroleum industry that in recent years has exceeded USD $100 billion in value (Government of Western Australia 2013).

The nature of offshore infrastructure, some of which lies several hundred kilometers away from the coast, demands a different level of advance warning, particularly with respect to personnel safety and offshore facility evacuation planning. The advanced plans of several consortia to deploy floating natural gas platforms (largest in the world), instead of the conventional gas riser technology, for gas delivery also imposes demand on accurate forecasting in a region where winds of up to 400 kph with seas of 30 m have been recorded (e.g., TC Olivia 1996). There is thus great interest in knowing how the statistics of tropical cyclone number, intensity, and landfall locations change in a warming climate. As a first step, we would like to investigate past changes in cyclone activities (e.g., the mean annual

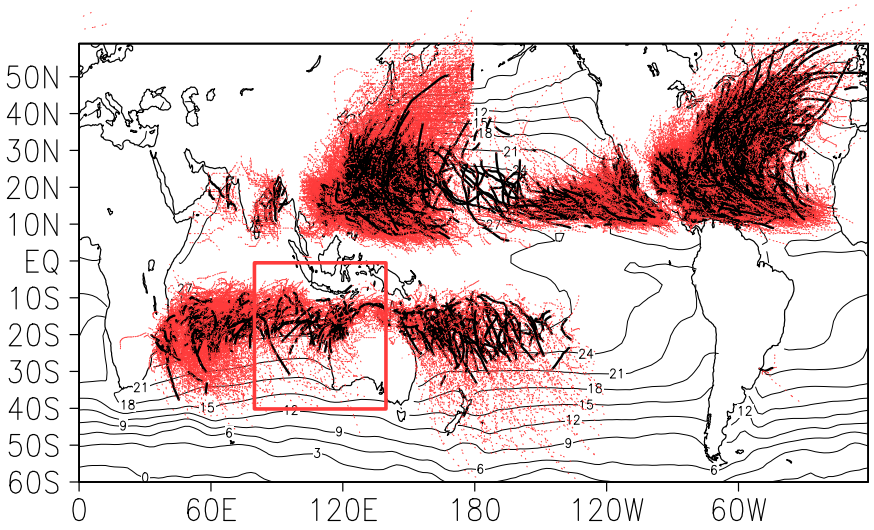


Figure 1. Global hurricane tracks from IBTrACs. Bold lines are category 4 and 5 TCs. Contour lines are annual-mean sea surface temperature over 1960–2010. Notice that ocean currents (e.g., Gulf Stream and Kuroshio) have high correlation with the mean TC tracks. On the other hand, cold upwelling currents and the associated unfavorable wind shear prevent the formation of TCs. For example, the presence of the Peru/Humboldt Current and Benguela Current hinder the TC formation in the southeastern Pacific and southeastern Atlantic oceans. The red box defines the NWA (equator–40°S; 80°–140°E) basin. We define NWA using this region because it contains the genesis and development locations of all documented TCs that landed on Western Australia.

frequency, the genesis and landfall locations, and track) and the large-scale environmental conditions linked to the formation and track of tropical cyclones, especially to investigate the mechanism that caused an observed shift of the landfall locations, and the occurrence of strong (category 3 or stronger) TCs.

In this study, the focus initially is on historical trends in TC numbers and intensities. Next, the TC genesis and decay positions are examined for trends in their longitudinal and latitudinal locations. The northwestern coast of Australia is subject to the impact of tropical cyclones primarily during the summer season (Burroughs 2003). The adjacent ocean regions, including the Arafura Sea, are frequently characterized by relatively high sea surface temperatures (SSTs $>$ 30°C) at this time of year. This region has significant shipping activities associated with the export of iron ore. In the Pilbara and Kimberley regions of NWA, there are particularly large investments in offshore infrastructures associated with the production of liquid petroleum and natural gas. With respect to the ocean environment, the Holloway Current is a particularly warm current that flows down the NWA coast during the summer months and ensures a supply of low-level moisture to systems approaching the coasts. Further, the Leeuwin Current, which is linked to the Indonesian throughflow and is supported by local precipitation, provides a further source of warm water moving poleward. While the Leeuwin Current is primarily a winter

current, it does flow all year and is characterized by low salinity water. Expectations are that the Leeuwin Current, in providing a flow of warm, more southerly waters, may have a role to play in supporting the development of those tropical cyclones that occur in late spring (November) and early autumn (March).

This makes this region a climatologically sensitive basin because the warming of the ocean surface may significantly change the genesis and longevity of the TCs (Knutson et al. 2010). Encouraged by the results from analyzing TC activities over NWA for 1960–2010, we also investigate possible future changes in TCs using simulations from a high-resolution climate model, the Geophysical Fluid Dynamics Laboratory (GFDL) High Resolution Atmospheric Model (HiRAM; Zhao et al. 2009; Zhao and Held 2010) simulation, and an advanced tracker scheme.

2. Data

Tropical cyclone observations at 6-h intervals were obtained from the International Best Track Archive for Climate Stewardship (IBTrACS; Kruk et al. 2010; http://www.ncdc.noaa.gov/oa/ibtracs/). To illustrate the physics responsible for changes in TC activities, we also use the NCEP–NCAR reanalysis products (Kalnay et al. 1996). The analysis archive covers the period from 1948 to 2012 and can be divided into three periods corresponding to the evolution of the major observing systems: the early years from 1948 to 1957, where very few upper-air observations were made; the rawinsonde era from 1958 to 1978; and the satellite era from 1979 onward. Data deficiencies in the early years made the analyses demonstrably less reliable compared to later years (Emanuel 2010; Kistler et al. 2001; Kossin et al. 2007). We thus restrict our historical analysis to the years 1960–2010, a period of reasonable data quality that is sufficiently long for a robust climate variability analysis. For example, Holland and Webster (2007) stated that tropical data since 1960 are of good quality and free of major observational bias.

To estimate future trends, a cyclone tracker scheme (to be detailed) is used to identify TCs from meteorological fields. High resolution (on the order of 10 km) is a prerequisite because a single TC is a mesoscale phenomenon. The GFDL HiRAM (Putman and Lin 2007), specifically C180 HiRAM2.1, simulations were chosen (over most PCMDI posted climate model simulations for the IPCC Fourth Assessment Report) primarily because of their fine horizontal resolution (~50 km) and the relevance to climate studies. The GFDL HiRAM has 32 vertical levels [one-third more than the GFDL Atmospheric Model version 2 (AM2) model, its predecessor] and covers the entire globe. It utilizes a cubed sphere dynamical core (Zhao and Held 2010) with 180 × 180 grid points on each face of the cube, resulting in grid sizes ranging from 43.5 to 61.6 km. The model includes numerous improvements in physical parameterization to facilitate simulation of the tropical atmosphere, including the Bretherton et al. (2004) shallow convection parameterization and the cloud physics closure. During the twentieth-century simulations, the lower boundary SSTs are observed sea surface temperature from the Hadley Centre Sea Ice and Sea Surface Temperature dataset (V1.1), interpolated to 6-hourly intervals. The climatological statistics of tropical cyclones simulated in this model, as well as the interannual variability in the model forced by observed SST, indicate that it can faithfully simulate the geographical distribution of storm genesis locations as well as seasonal cycles and interannual variability of tropical

cyclone frequency for the major basins (e.g., Zhao and Held 2010). For twenty-first-century projection, we only examine the IPCC Special Report on Emissions Scenarios (SRES) A1B emission scenario runs.

3. Methods

A range of statistical techniques is employed to determine trends in TC activity. Here, TC activity is taken as mean annual frequency, and the genesis and decay location changes in a TC basin. The techniques are not new and therefore are described only briefly below.

3.1. TC tracker

Global climate models can provide useful information about the sensitivity of tropical cyclone climate to increased greenhouse gases (Broccoli and Manabe 1990, 1992; Bengtsson et al. 2007). An automated tropical cyclone detection scheme is a prerequisite for the analysis of TCs in climate model simulations. The resolution of climate models still is too coarse to simulate TC vortices in detail. Hence, to identify a TC-like vortex in climate model simulations, the tracker must apply a number of criteria to identify candidates from a wide variety of disturbances and then follow the centers to build up a full track. As described by Walsh (2004), a typical tracker starts by locating a localized minimum in surface pressure or maximum in cyclonic vorticity to identify a potential cyclone. Once identified, the system is then filtered using preset thresholds of maximum wind speed, vorticity, duration, and some measure of the presence of a warm core. In addition, some studies based on high-resolution models have utilized criteria based on genesis location, surface pressure anomaly, and a measure of structure in terms of vertical variation of tangential maximum wind speed and/or horizontal temperature gradients. All of these criteria, and particularly structure and intensity, are strongly dependent on model resolution (Oouchi et al. 2006; Stowasser et al. 2007; Rotunno et al. 2009) and to some extent on model physical parameterizations (e.g., Walsh et al. 2007). Differentiating maximum winds and core details requires a few kilometers resolution, and spiral bands and realistic asymmetries need 10-km resolution, while the warm core and well-defined eye need only 50-km resolution. The critical values in a tracker thus vary according to atmospheric fields from models of different resolution. Also, TCs in different basins have very different morphologies (Figure 1). For example, durations in the southern Indian basin are usually shorter because of the lower sea surface temperature and stronger longitudinal gradients. Similarly, the maximum attainable wind speeds and vorticity (negative in Southern Hemisphere) are also very different. In this study, the criteria are similar to those employed by Ookuchi et al. (2006), which were designed specifically to extract TCs with genesis in the tropics and to avoid the extraction of unwanted midlatitude cyclones.

3.2. TC criteria used by the tracker

The processing methods used by the tracker to identify storm centers include the following:

1) The 850-hPa relative vorticity exceeds a threshold value of 3×10^{-5} Hz (in the Southern Hemisphere a negative threshold of the same magnitude is used).
2) The maximum near-surface (10 m) wind speed in a centered 350-km box exceeds the wind speed threshold of 12 m s^{-1} (note that this is lower than the 17 m s^{-1} criteria from the observational definition of TCs because of the fact that climate model usually simulates a weaker circulation than reality).
3) The sea level pressure is the minimum in the box.
4) The temperature anomaly averaged over the 350-km box and three pressure levels (300, 500, and 700 hPa) exceeds the temperature anomaly threshold.
5) The local temperature anomaly averaged over the box is positive at all three pressure levels (300, 500, and 700 hPa).
6) The local temperature anomaly, averaged over the box at 300 hPa, is greater than at 850 hPa.
7) The mean wind speed averaged over the 350-km box is larger at 850 hPa than at 300 hPa.
8) The grid points representing the center of storms that obey all the above criteria are connected if they are less than a certain distance from the center of the previous time step analyzed. This distance is defined by the frequency of the output of the model. For 6-hourly outputs, two grid points are used in longitude and/or latitude, while for daily output, four grid points is the maximum distance.
9) In addition to the warm-core criterion of Bengtsson et al. (2007) to further exclude possibilities of including subtropical cyclones, a cyclone-phase technique (Hart and Evans 2001; Hart 2003; Evans and Hart 2003) is implemented that provides a comprehensive measure of the vertical thermal structure of low pressure systems. This is in response to the fact that only stipulating that the maximum wind speed within the 350-km box of the storm center is greater at 850 hPa than at 300 hPa, and the temperature anomaly at 300 hPa is larger than that at 850 hPa (Horn et al. 2014) is insufficient to fully differentiate tropical and nontropical systems.
10) The storm lasts for at least 36 h. Because of the volume of the high-resolution model output, it is usually processed in many segments in time [e.g., a netCDF file for 1 day of the NCAR–Nested Regional Climate Model (NRCM) for all the variables, and a netCDF file for 1 year of one single variable of the GFDL HiRAM]. For those TCs that span two processing periods, our postprocessing scheme properly rearranges the identified vortices to align those belonging to one TC.

3.3. Statistical analysis methods

To assess the trend in TC activity in the past 50 years and climate model–projected changes in the future, several methods were employed. In the following

discussion, when we say there is a trend we mean that the linear trend of a time series is positive at 95% confidence based on the Mann–Kendall test (Mann 1945; Kendall 1970; McLeod et al. 1991). Following the track analysis by Camargo et al. (2007a,b), the cluster analysis of the genesis and landfall positions of TCs involves a multivariate kernel density estimation (KDE) method, with a Gaussian kernel. The univariate KDE approximates the probability density function of a point x as

$$f(x) = \frac{1}{n}\sum_{i=1}^{n} K_h(x - x_i), \tag{1}$$

where n is the number of observations, h is a smoothing variable (the bandwidth), x_i are observations/realizations of random variable x, and K_h is a kernel function. There are a number of possible choices of kernel function. For this study the Gaussian (normal) kernel is used. It is defined as

$$K_h(x - x_i) = \frac{1}{h\sqrt{2\pi}} e^{[-(x-x_i)^2]/2h^2}. \tag{2}$$

A two-dimensional KDE can be represented by

$$f(x) = \frac{1}{n}\sum_{i=1}^{n} [K_{h_1}(x^{(1)} - x_i^{(1)})][K_{h_2}(x^{(2)} - x_i^{(2)})], \tag{3}$$

where $x = (x^{(1)}, x^{(2)})$, a two-dimensional extension of the random variable representing the latitude and longitude of the TC landing locations and with separate bandwidths for each dimension. Here, multiple bandwidth pairs (h_1, h_2) were used for comparison, as well as the bandwidth pair determined by the normal reference rule for a multivariate KDE given in Scott (1992):

$$h_j^* = \left[\frac{4}{n(d+2)}\right]^{1/(d+4)} \sigma_j, \quad j = 1, 2, \tag{4}$$

where σ is the sample standard deviation (a vector for multidimensional x), n is the number of training examples, and d is the number of dimensions. In this study, $d = 2$ (i.e., the component index j varies from 1 to 2) and thus

$$h_j^* = \left(\frac{1}{n}\right)^{1/6} \sigma_j = n^{-1/6}\sigma_j. \tag{5}$$

4. Results

In the first half of this work, we investigate the TC activities over the past 50 years in the hope that changes of TC activities over this period can at least give us a hint of future changes since, based on independent evidence, the past 50 years experienced rapid climate change.

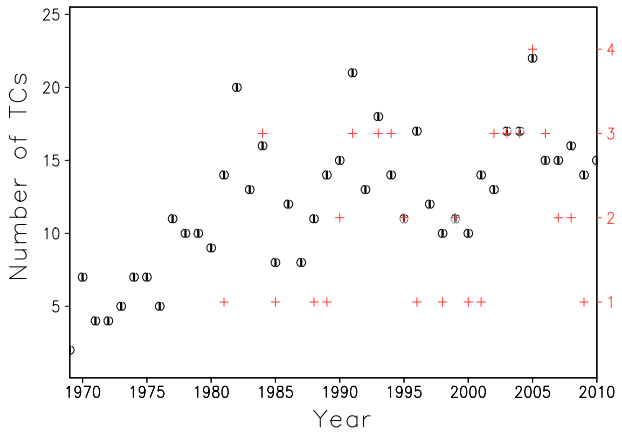


Figure 2. Time series of strong TC (reaching wind speed greater than 50 m s^{-1}) occurrence globally (black marker) and for NWA basin (red cross) over 1970–2010. For the global time series, there is a positive trend. For NWA, however, strong natural variability prevents detection of statistically robust trends.

4.1. TC activities during the past 50 years

Figure 2 presents time series of strong (reaching wind speed greater than 50 m s^{-1}) TC occurrence globally (black marker) and the NWA basin (red cross) over 1970–2010. For the global time series, there is a positive trend. For NWA, however, strong natural variability prevents detection of statistically robust trends. We also notice that the Indian dipole and southern annular mode all have clear bearings on the occurrence of strong TCs over NWA (figure not shown). If those tropical cyclones with central pressure lower than 930 hPa (categories 4 and 5) are defined as strong TCs, it is noticed that 40% reached category 3 during 1960–85 period, and this proportion increased to 60% for the 1985–2011 period.

Figure 3 shows the mean tracks of landfall TCs over 1960–85 (red) and 1985–2010 (green) and their clustering centers (markers of the same color). The mean track is obtained by averaging the longitudes of all landed TCs for every 0.5° latitude interval from 35° to 10°S. It is noticeable that the mean track has shifted inland (to the east) by about 1° (not shown for clarity), and this signal is statistically significant. Landfall cluster centers are obtained using the above-mentioned KDE method. Over the region of interest, there are actually two disconnected "hot spots" [defined by the two boxes labeled with NWA and North Australia (NA) in Figure 3]. The northeast shift of the cluster center over the 1985–2010 period compared with the 1960–85 period occurs because there are relatively more landfalls in the NA subregion. Because of the lack of remote sensing observations for the first period, there is usually a lack of track records over the ocean (only the landfall records are available in the IBTrACS). Thus, the mean track shift cannot be taken too literally. Because historically this region is also sparsely populated, chances are there are missing records, especially for the first period (1960–85). This could be reflected in the total number of landfall TCs in the record: 29 in the

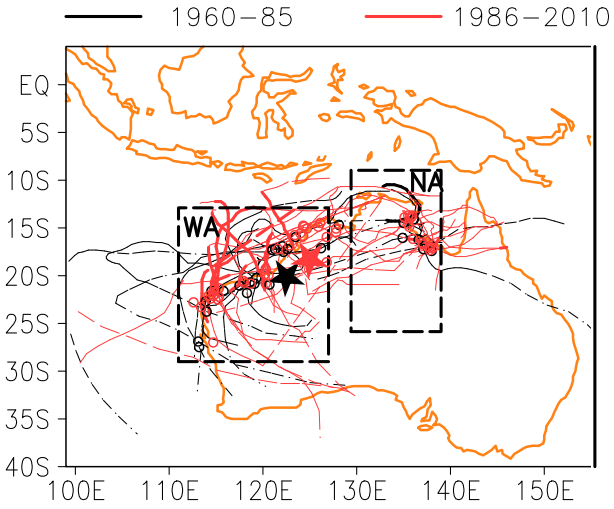


Figure 3. Tracks of landfall TCs over 1960–85 (black) and 1986–2010 (red) and their clustering centers (stars of the same color). Cluster centers are obtained using the KDE method. The landfall locations are labeled with round marks of the same colors as the tracks.

first period and 51 in the second period. However, the shift in the cluster center is robust to data scarcity. In the second period, relatively fewer landfalls occurred in the NWA and more landfalls occurred in the NA subbasins. This is related to the origin of the landfalling TCs over the region of interest. The majority is generated in the warm pool of the Arafura Sea north of Darwin (e.g., the severe Tropical Cyclone Olivia 1996). Also, there is regrowth from remnants of TCs that developed in the South Pacific basin (e.g., Glenda 2006). Glenda is a characteristic redevelopment of a cyclonic remnant (of TC Larry 2006) after passing over a warm ocean surface, which is clearly shown in the potential vorticity map generated from reanalysis data (not shown). While the Olivia-like TCs make landfall over NWA, the Glenda-like TCs can make landfall either over NA or NWA. The shift (toward northeast) of the cluster center of the landfall TCs resulted from an increase (in percentage) of Glenda-like TCs in the 1985–2010 period. If only the categorical TCs (TCs that reached sustained surface winds of 17 m s^{-1}; Henderson-Sellers et al. 1998) are considered, the cluster center shifts to the NWA side instead.

The NWA basin is sensitive to climate change. The 500-hPa geopotential height (Figure 4) has expanded poleward, and this is a robust signal of atmospheric warming. Because the total air mass has not changed, the only mechanism that can globally raise the 500-hPa geopotential height contour is thermal expansion of the atmosphere. The figure panel focused on our region of interest, but the poleward expansion of the contour lines of geopotential height is a global phenomenon. At the same time, the area-mean annual-mean SSTs (Figure 5a) have increased steadily over the past 50 years (Figure 5b). Although there is no direct unanimous correspondence between SST and TC activities (other factors such as vertical wind shear and synoptic disturbances may also play critical roles in the formation and growth of TCs), the primary factors limiting the TC longevity for the NWA basin

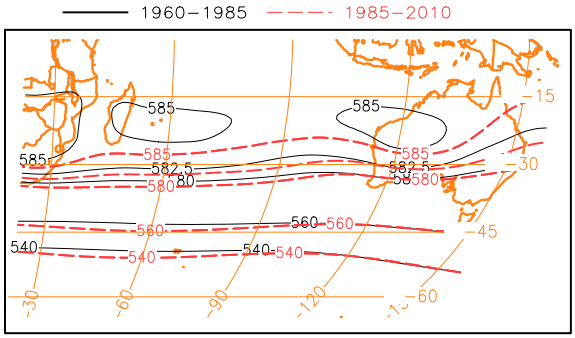


Figure 4. Signs of climate warming during the past 50 years; changes of 500-hPa geopotential heights (decameters or 10 m) for austral summer. The Robinson projection is used.

seems to be the relatively low SST for the genesis and development areas (region confined by curved box in Figure 5a). If the increasing pattern of SST (Figure 5b) continues, it will indicate that the NWA TC basin is a climatologically sensitive basin. In addition, the warm alongshore Leeuwin Current provides favorable conditions for TC landfall.

To investigate future changes in TC activities, we investigate the TCs identified by the tracker from the climate model–simulated atmospheric fields. We would like to find which signal, identified in analyzing the historical IBTrACS data, is persistent in a warming climate. As mentioned above, no GCM model at present can accurately simulate hurricane intensity, especially for major hurricanes (category 3 and higher, with maximum wind speed greater than 50 m s^{-1}), as can be seen in Figure 1 of Zhao et al. (2009). We thus cannot take the GFDL HiRAM–simulated future hurricane intensity in a warming climate at face value. The changes in intensity distribution, however, may have qualitative value. Thus, the following analyses performed are in a relative sense identifying the first-order trend in TC activities. The model-simulated TCs are known to be weaker than reality (as a common shortcoming among GCM models). Zhao and Held (2010) proposed a statistical method to adjust the probability distribution of intensity (maximum storm life mean wind speed). The same techniques are used here so that the traditional classification of TCs (categories 1 to 5) is retained.

4.2. Future TC activities in model simulations with A1B scenario

To assess future changes in TC tracks over the NWA, we use the ~50-km grid spacing GFDL HiRAM with SST provided by a coupled GFDL CM2.1 run under the IPCC's SRES A1B emissions scenario, which is a commonly employed moderate development scenario (http://www.ipcc-data.org/ar4/scenario-SRA1B-change.html). The NWA TC basin study carried out here uses 6-hourly output, for the projection period 2000–60, from the GFDL HiRAM. The SRES A1B future scenario is used to calculate trends in TC numbers and intensities. Differences are computed between a control model run (CNTRL) with fixed CO_2 levels for the

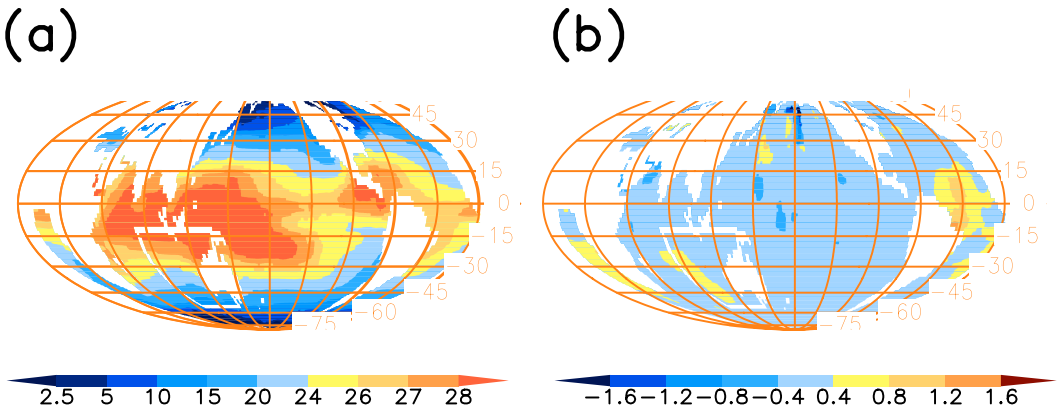


Figure 5. (a) Climate mean SST and (b) changes expressed as SST (1985–2010) minus SST (1960–1985). The NWA is a region of apparent SST increase (>0.5°C), exceeded only by the southern Atlantic Ocean off the Brazilian coast. SST of the western boundary of the NWA basin is relatively cooler than other TC basins (the area above 25°C is only 1/8 that of the west Pacific Ocean basin). Mollweide equal area projection is used in the display for its accurate proportion in area, globally.

years 2000–60 and a projection using the enhanced CO_2 A1B scenario (EGHG) for the same period.

The GFDL HiRAM resolves basic features of tropical cyclones necessary for a tracker to work: quasi-axisymmetric shape, wind speed maximum just above the planetary boundary layer, and a salient upper-level (300 hPa) warm core, without any attached ‘‘front.’’ However, like all other climate models, it still cannot reproduce observed cyclones or TC intensity for comparison with observations (Figure 6). The NCAR–NRCM global tropical belt (45°S–45°N) model ~36-km resolution, forced by NCEP–NCAR reanalysis as meridional boundary conditions and AMIP SST (Hurrell et al. 2008) during twentieth-century run and CCSM4 boundary conditions for scenario runs of the twenty-first century, is valid for simulating TCs (figures not shown). In the following discussion, unless otherwise noted, consensus results from GFDL HiRAM and NCAR–NRCM belt models are given.

4.2.1. TC activity: Centroids, frequencies, and intensities

Although there have been significant improvements in physical parameterizations and refinements in horizontal resolution during the past two decades, the assertions of Henderson-Sellers et al. (1998) that ‘‘the tropical cyclone–like’’ vortices in the climate model simulations cannot be directly comparable with archived TC observations, especially in intensity, are still valid. This caveat in climate model simulations of TCs also explains the experimental design in this study, namely, the comparisons between the CNTRL and EGHG runs, rather than a direct comparison of the EGHG run with IBTrACs. We believe that this is a fair comparison, and the results are reliable and robust to climate model

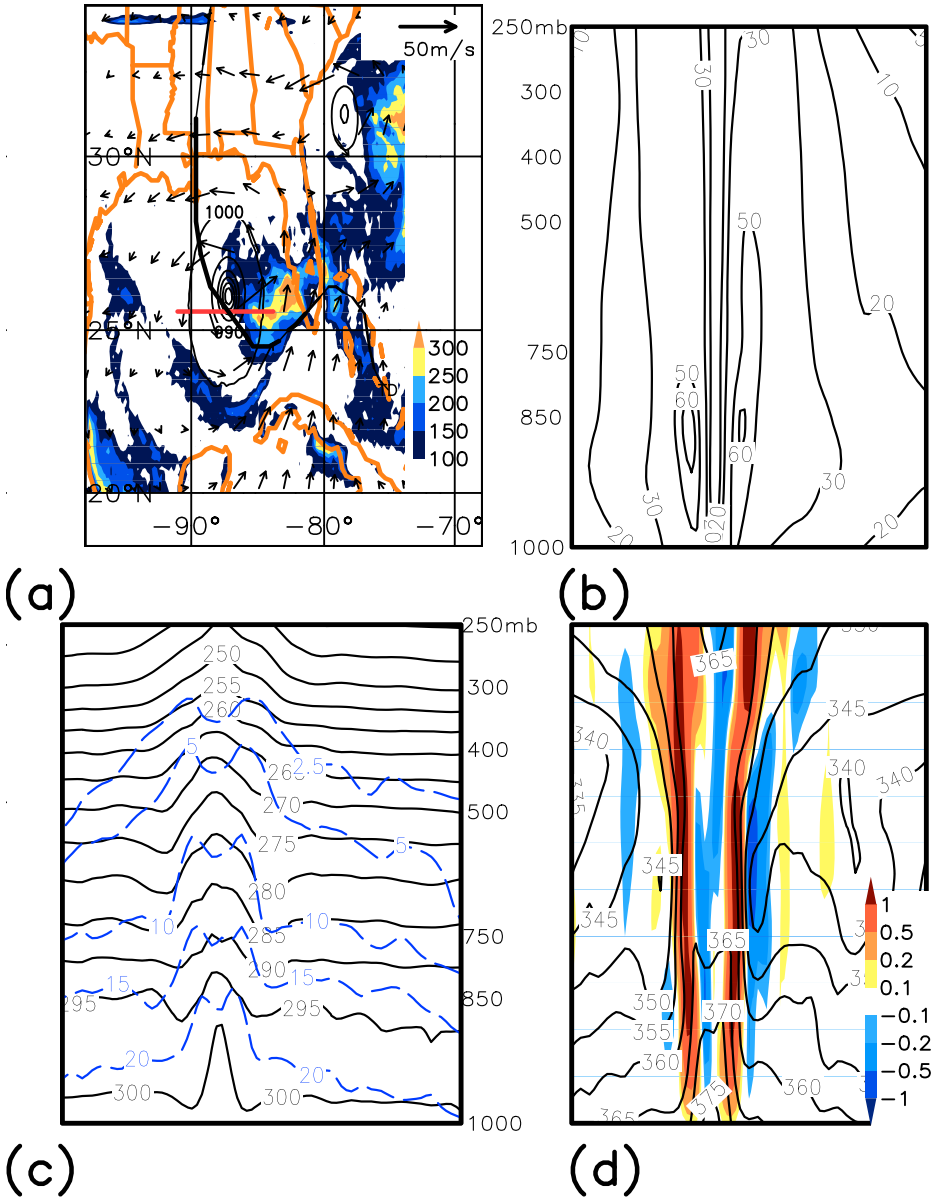


Figure 6. Structure of a simulated Atlantic basin tropical cyclone from the GFDL HiRAM CNTRL simulation. Typical features necessary for the tracker (to detect TCs) are resolved, including (a) quasi-axisymmetric shape, (b) wind speed maximum just above the planetary boundary layer (~900 hPa), and (c) an upper-level warm core. In (a), contour lines are surface level pressure (hPa), and shades are precipitation (accumulated total amount in the 6-h period; mm). (b) Wind speed in a cross section along 26°N (marked as red line in (a)). (c) The temperature (K; solid line) and specific humidity (g kg^{-1}; dashed line) in the same vertical cross section. In (d), shading is vertical motion (m s^{-1}). The contour lines are equivalent potential temperature (K). Model time is 28 Aug 2005. The model provides a consistent picture of the warm-core structure of a mature tropical cyclone.

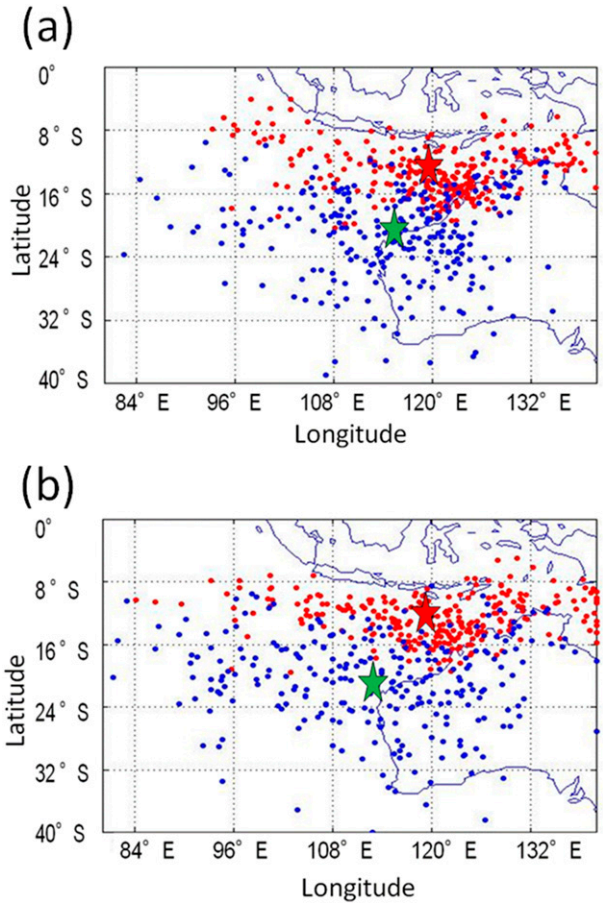


Figure 7. (a) The locations of the CNTRL start (red) and end (blue) points of tropical cyclones in the NWA TC basin. Centroids of the start and end points are shown as red stars (approximately 13°S, 120°E) and green (approximately 21°S, 114°E) stars, respectively. (b) As in (a), but for the SRES A1B scenario (EGHG). Centroids of start and end points are shown as stars at approximately 12°S, 120°E and approximately 20°S, 112°E, respectively.

selection. In Figures 7a and 7b, the start (red) and end (blue) positions of all TCs for the 60-yr period 2001–60 are shown for the CNTRL and EGHG datasets. The centroids of the start and end positions are also marked by red and green stars, respectively. Table 1 summarizes the centroid latitudes and longitudes for all cases.

In Figures 8a and 8b, the annual and pentad frequencies of all TCs in the NWA basin are shown for the CNTRL model, over the full period 2001–60. Of particular interest is the statistically significant downward trend over the period, shown by the linear trend lines in each figure. Similarly, Figures 9a and 9b, for the EGHG annual and pentad frequencies also reveal a downward trend over the full period. In marked contrast, Figures 10a and 10b show that the number of severe TCs, defined as having central pressures of 960 hPa or below, have a downward trend for the

Table 1. CNTRL and EGHG start and end latitude/longitude centroid positions.

CNTRL (start)	CNTRL (end)	EGHG (start)	EGHG (end)
13.22°S, 120.05°E	20.84°S, 115.48°E	12.61°S, 120.51°E	20.64°S, 112.99°E

CNTRL run but an upward trend for the EGHG run. In summary, the CNTRL and EGHG model projections have a similar downward trend in TC numbers but differ in the number of projected severe NWA TCs occurrence frequencies. These findings are consistent with those for other TC basins (Wu and Wang 2004; McDonald et al. 2005; Bengtsson et al. 2007; Stowasser et al. 2007; Yokio and Takayabu 2009; Murakami and Sugi 2010; Murakami and Wang 2010; Murakami et al. 2011).

4.2.2. Statistical significance of differences in EGHG and CNTRL TC mean start and end positions

The finding in section 4.2.1—that the centroids of the start and end positions differ between the CNTRL and EGHG model runs—is tested for statistical significance by using two nonparametric permutation tests. Both a bootstrap method and a permutation test with replacement were applied. As the findings are similar, only the results of the permutation test with replacement are presented here. The permutation method was applied to both the difference in mean centroid positions and also to the difference in centroid position variances. Second, a permutation test was performed on the differences in variance between control and EGHG datasets. The permutation test computed a one-sided p value with the null hypothesis that the differences in the mean positions, and also in the variance, between the longitude/latitude of the EGHG run was less than or equal to that of the CNTRL run. If the

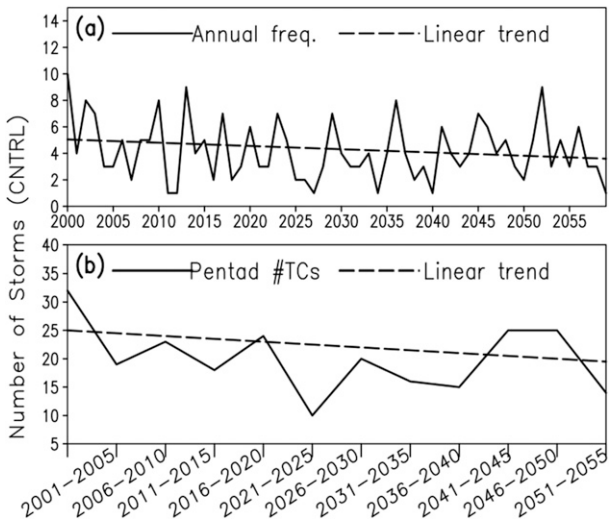


Figure 8. (a) The annual frequency of tropical cyclones in the NW TC basin region for the CNTRL experiment for the period 2001–60. The linear trend line also is shown. (b) As in (a), but for pentad averages.

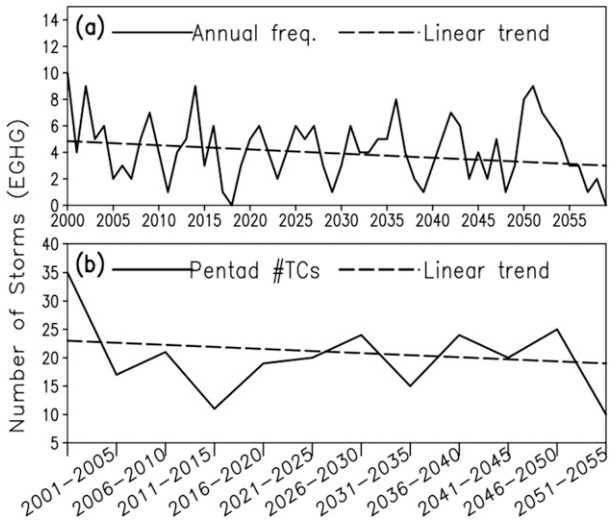


Figure 9. As in Figure 8, but for the EGHG experiment.

null hypotheses are false, the mean and variance in the EGHG run are significantly greater than for the CNTRL run.

For the null hypothesis that the mean (centroid) latitude of the EGHG start positions (13.22°S) does not differ from the CNTRL mean latitude start positions (12.61°S), as shown in column 1 of Table 2, the p value is 0.0118. The null hypothesis therefore was rejected and there is a statistically significant difference between the mean start latitudes, namely, that the mean of the EGHG latitude start positions is less than the mean of the CNTRL latitude start positions (i.e., the mean EGHG start latitude is significantly equatorward of the mean CNTRL start latitude). This seems in discord with the fact that the subtropical high has an expanding trend with global warming. Careful examination of the atmospheric fields indicates that the subtropical highs are more fractured and there are many discontinuous belts of relatively low pressure nested inside them. This disagreement with the findings of Lavender and Walsh (2011) also is likely due to the weaker criteria for defining a TC (i.e., identifying 6–10 more TCs in the CNTRL and EGHG runs than the Lavender and Walsh scheme) applied here.

A second null hypothesis, comparing the mean longitude of the EGHG end positions with those of the CNTRL, produced a p value of 0.010 18 (column 4 of Table 2), indicating that the mean of EGHG longitude end positions was significantly less than the mean of the CNTRL longitude end positions (i.e., the mean EGHG end longitude is significantly west of the mean CNTRL longitude).

However, the two other null hypotheses concerning the differences in mean positions of the start longitudes and the end latitudes of the EGHG dataset, as shown in columns 2 and 3 of Table 2, are not rejected at the 5% significance level. That is, the mean start longitudes (and end latitudes) of the EGHG locations are not significantly different.

Turning to the variances in the CNTRL and EGHG positions, the p value of 0.9979 in column 1 of Table 3 indicates that the variance of the EGHG is not

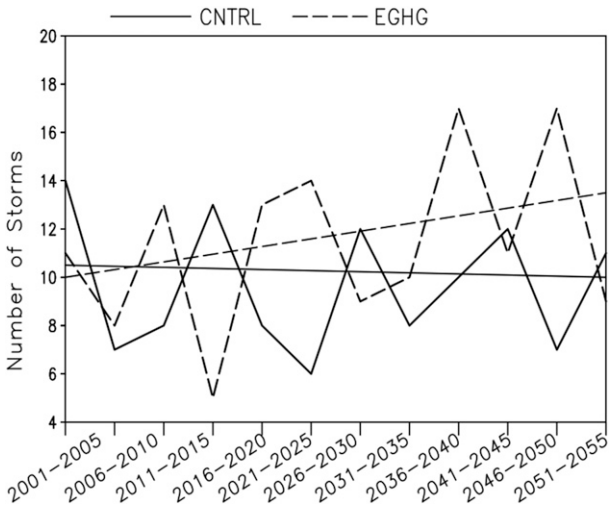


Figure 10. The number of severe tropical cyclones (solid lines for CNTRL and dashed lines for EGHG experiments), by pentad, for the period 2001–60, with the linear trend line in same style.

significantly less than or equal to that of the CNTRL experiments. The p value of 0.4446 in column 2 of Table 3 also shows that the null hypothesis cannot be rejected. However, in the case of the start and end longitudes, the p values of 0.0196 and 0.0012 in columns 3 and 4 of Table 3 imply that we can reject the null hypotheses at the 5% significance level and therefore conclude that the variances of the start and end longitudes of the EGHG projections are significantly larger than the CNTRL variances.

4.2.3. KDE analysis

The KDEs were calculated for the CNTRL start and end positions (Figures 11a,b) and the EGHG start and end positions (Figures 12a,b) for the 2D bandwidths of Equation (5). Figure 12 is the same as Figure 11, except that the bandwidths are varied. Figure 12 has smaller bandwidths (1.5, 1.5) and Figure 11 has generally wider bandwidths. For TC pattern classification (Kim et al. 2011), the KDEs also were calculated for a range of bandwidths. Theoretically, for density-based clustering analysis, the narrower the bandwidth, the more likely more cluster centers can be identified from the datasets. The effectiveness of kernel density estimation also depends on the bandwidth selection. However, the KDEs all led to the same conclusion that just one cluster is present, although in some cases it likely is a

Table 2. The p values of the significance of the differences in CNTRL and EGHG start and end latitude/longitude centroid positions.

CNTRL–EGHG Start lat centroid	CNTRL–EGHG End lat centroid	CNTRL–EGHG Start lon centroid	CNTRL–EGHG End lon centroid
0.0118	0.3280	0.3097	0.0108

Table 3. The *p* values of the significance of the differences in CNTRL and EGHG start and end latitude /longitude variances.

CNTRL–EGHG (start) lat variance	CNTRL–EGHG (end) lat variance	CNTRL–EGHG (start) lon variance	CNTRL–EGHG (end) lon variance
0.9979	0.4446	0.0196	0.0012

disjointed cluster. This finding that there is only one cluster present in the NWA TC basin is supported in a recent study of TC basins in the Southern Hemisphere that show the presence of only one TC track cluster in the NWA TC basin (Y. Wang 2011, personal communication).

The number of storm days is a valid alternative parameter to represent tropical cyclone activities. The number of storm days has been used by many studies in the past (e.g., Wang et al. 2009). It provides an overall picture of the entire life cycle of tropical cyclone activity for a particular basin. While it is true that the model resolution is still too coarse to resolve tropical cyclones, the comparison of the enhanced GHG scenario with the control experiment still

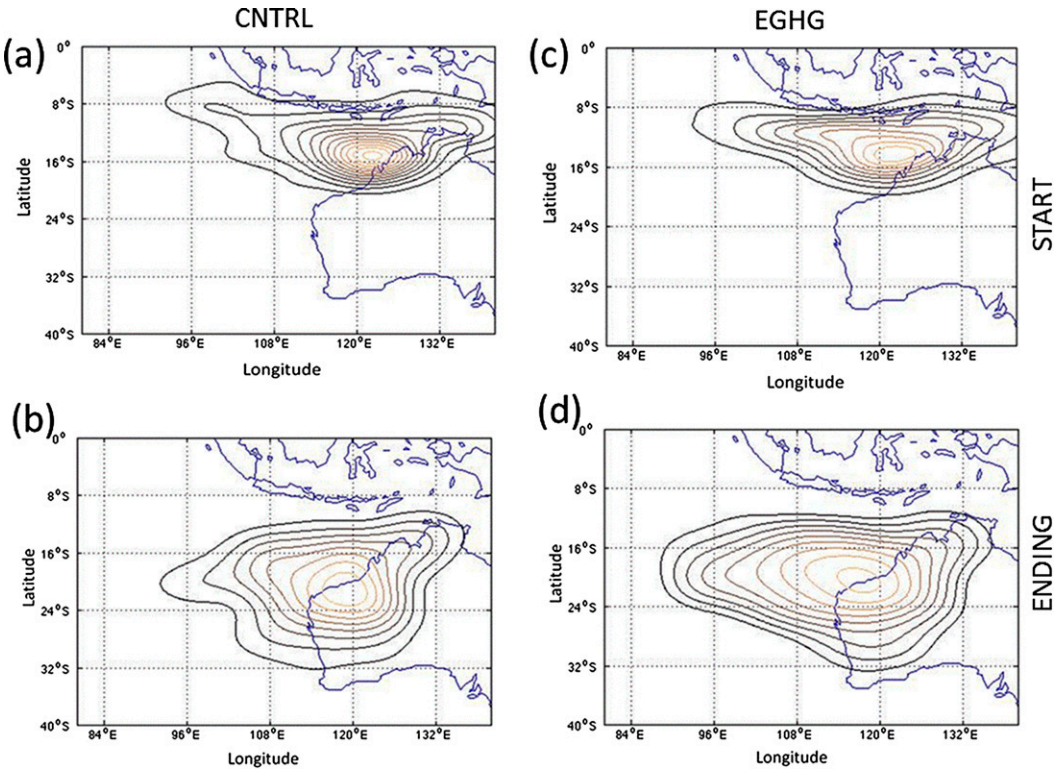


Figure 11. The KDE contours for the CNTRL (a) start and (b) end points. The normal, reference 2D bandwidths of (3.9501, 1.2903) and (4.0917, 2.2958) are used to generate the KDEs. (c),(d) As in (a),(b), but for the EGHG experiment, which has bandwidths for the start and end points of (4.6157, 1.0922) and (4.9775, 2.3167), respectively.

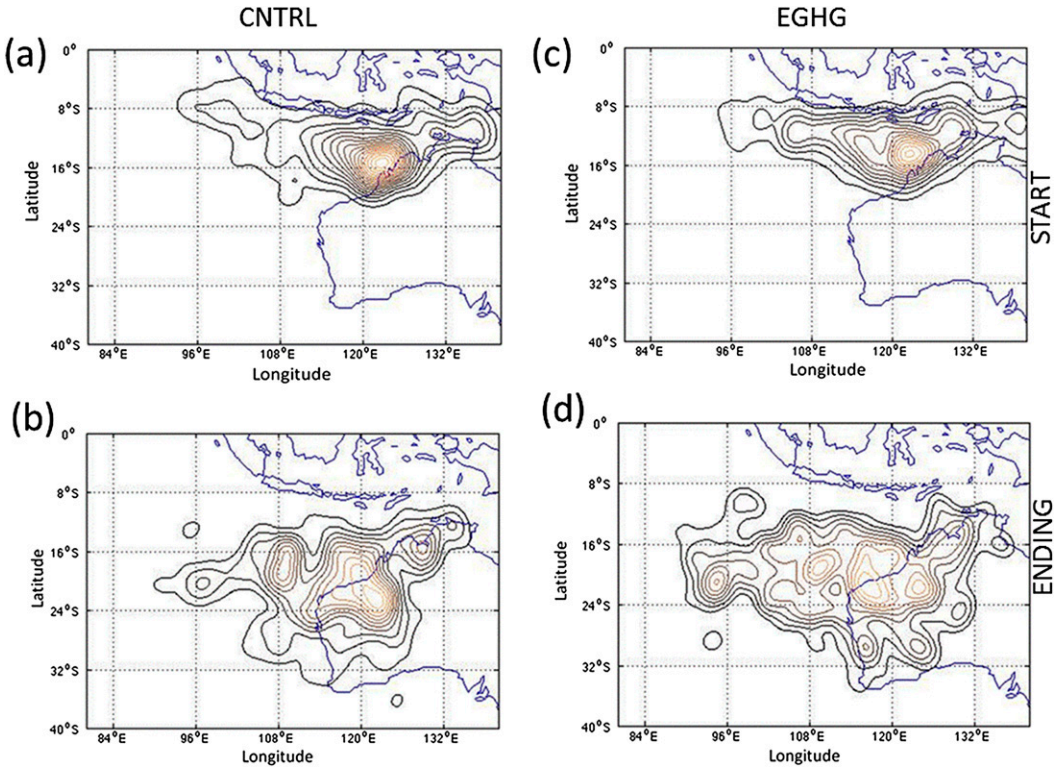


Figure 12. As in Figure 11, but with a 2D bandwidth of (1.5, 1.5). (a),(b) Control experiments. (c),(d) The corresponding EGHG experiments.

shed light on the impact of climate warming on TC activity. There is significant increase (95 percentile) in storm days for the NWA TC basin, in agreement with Wang et al. (2009). This increase is mainly due to the increase in TC genesis. Steering currents do not change significantly as the climate warms. The reduction of winds due to reduced latitudinal gradients (polar amplification of climate warming) in the air temperature mainly is significant for the midlatitudes and only affects the translation speed of TCs after reaching their turning points.

Because extreme events are very relevant to the safety of offshore oil platforms, the probability distribution of maximum wind speed also is examined. The Zhao and Held (2010) statistical augmentation is applied to the climate model–simulated atmospheric parameters. The bin interval for wind speed is $0.5\,\mathrm{m\,s^{-1}}$. The associated histogram is shifted systematically toward more extreme events. For example, there is a ~2% increase in category 3 and above (maximum sustainable winds reaching $>45\,\mathrm{m\,s^{-1}}$) TCs for EGHG simulations than for the CNTRL simulations. Ren et al. (2014) defined an objective measure of total kinetic energy of a TC to permit interbasin comparisons. A histogram of the peak values of the total kinetic energy was plotted (figures not shown). The peak value shifted from 3.5×10^6 to 3.57×10^6 TJ, a robust signal indicating increased destructiveness.

5. Discussion

In the past 50 years, there are statistically significant inland shifts in TC tracks over the NWA region. Although the wind speed of a cyclone reduces dramatically after landfall, the moisture residual can be picked up by midlatitude disturbances and produce a significant amount of precipitation (Wang et al. 2009). For Western Australia, these TC remnants are passing over a climate zone comprising a mixture of perennial and seasonal vegetation cover. The perennials may likely adapt to the plant available soil water deficit associated with the annual precipitation pattern (the primary precipitation for this region is the wintertime precipitation occurring after the northward shift of the subtropical ridge line). The increased precipitation from TCs is a supplement that will broaden the precipitation distribution curve on the annual-mean precipitation time series. Since water is a limiting factor for the perennial–seasonal ecosystem, in analogy to the Savannah system investigated by Eagleson (1982) and Eagleson and Tellers (1982), noticeable effects on the ecosystem balance (e.g., the observed dieback of perennial and flushing of seasonal plants) of NWA might be expected.

The NWA basin is also found to be sensitive to climate change. Future changes in TC activity in climate model projections over the northwest Western Australian TC basin were carried out for the period 2000–60. Projections from two coupled global climate models were assessed. One was a control run (CNTRL) that had CO_2 levels held fixed at year 2000 values. The other model run (EGHG) had enhanced CO_2 levels from the moderate IPCC SRES A1B future scenario. The A1B scenario is a commonly employed moderate development scenario. The main assumptions are that of a "future world of very rapid economic growth, global population that peaks in mid-century and declines thereafter, and the rapid introduction of new and more efficient technologies" (https://www.ipcc.ch/ipccreports/tar/wg1/029.htm#storya1). The results of this study are important because any significant trends in TC activity, and/or changes in the locations of the TC genesis and decay points, will have major consequences for the land-based coastal and offshore operations over northwest Western Australia.

First, the projected trends in mean annual frequencies and intensities were compared. It was found that there was no significant difference in the mean numbers of TCs between the CNTRL and EGHG projections, but there was a notable difference in the mean intensities, with the EGHG TCs being more intense at the 95% statistical significance level. The conclusion, which potentially is critical, is that it is likely that for the NWA TC basin, TCs will not change in number but will be significantly more intense. This intensity trend is qualitatively consistent with recent studies for Atlantic hurricanes (e.g., Bender et al. 2010; Knutson et al. 2010), which suggested that warmer climate likely leads to more very intense hurricanes. The claimed overall decrease in frequency may not be applicable globally though.

Second, the locations of genesis and decay points of the CNTRL and EGHG projections were compared. The results from a nonparametric permutation test revealed statistically significant differences between the projections for both the genesis and the decay locations. The importance of this finding is that the TCs will follow significantly different paths, with the EGHG TCs starting more equatorward than the CNTRL TCs, extending farther poleward and having a greater westward

longitudinal spread, thereby having a greater impact on coastal and inland Western Australia.

Third, a cluster analysis was carried out using a kernel density estimation (KDE) approach. The KDE method showed there was only one TC cluster, but the cluster appears to be disjointed. It was also found that there is a large scatter in the EGHG genesis and decay points when compared with the CNTRL runs and that, consistent with the second finding, the EGHG genesis points are shifted poleward by about 2° of latitude, while the decay points move westward by about 5° of longitude.

6. Conclusions

In this study, the focus initially is on trends in TC numbers and intensities. Next, the TC genesis and decay positions are examined for trends in their latitudinal and longitudinal locations. During the past 50 years, over the NWA TC basin, the cluster center of the landfall locations moved inland, primarily due to the expansion of the subtropical high. There are two source regions for the landfall TCs in this basin: those originating in the Arafura Sea and those redeveloping after landfall in Queensland. The shift of the cluster center is also due to the relative increase in the redevelopment type of TCs. If the A1B scenario is realized, there will be statistically significant changes in the cluster centers of the genesis/landfall locations. It is confirmed that, for the region of interest, more severe TCs (with minimum central pressure less than 960 hPa) become more frequent. These TCs possess more rapid intensification and quicker formation, leaving reduced warning issuance time for emergency services. This is counterintuitive because there clearly are fewer projected TCs in the future warming climate than at present, if the SRES A1B emission scenario is realized and all categories of TCs are counted.

There are numerous studies of other TC basins projecting the effects of future climate on SSTs based on increased carbon dioxide scenarios. Globally, the most studied TC basins are the Atlantic Ocean and the western North Pacific (WNP) Ocean. Although they are TC basin dependent, in general these projections show an increase in intensity and a decrease in TC number. However, the TC basin inconsistencies between the various model projections are such that the activity in each TC basin should be examined in detail. This study complements TC research for a less well-investigated basin. TC activities are controlled by large-scale environmental dynamics in a complicated way. More precise formulations of the mechanisms for such a trend will be examined in future work. Specifically, the effects of Madden–Julian oscillation and ENSO modulation on TC activities (e.g., Hall et al. 2001; Chand et al. 2013) will be examined for TCs of the NWA basin.

Over the past decade, the WNP has been the focus of many future projections in TC activity (see, e.g., Wu and Wang 2004; McDonald et al. 2005; Bengtsson et al. 2007; Stowasser et al. 2007; Yokio and Takayabu 2009; Murakami and Sugi 2010; Murakami and Wang 2010; Murakami et al. 2011). One of the key findings of Murakami et al. (2011) is that projected changes in TC activity, including TC frequency, are linked closely with location changes in TC genesis. In marked contrast, few studies have focused on the NWA TC basin (e.g., Broadbridge and Hanstrum 1998; Goebbert and Leslie 2010), and little is known about possible

trends in projections of TC activity in this region. Historically this is because of the small population of NWA. However, in recent years the Australian economy has been heavily biased toward resources with iron ore and oil and gas dominating production and expert earning. The total value of mineral and petroleum sales from just Western Australia was AUD $102 billion in 2012–13. The value of annual oil and gas production nationally in 2012–13 was approximately AUD $25 billion of which some AUD $22 billion was from the NW Western Australia region. The impact of tropical cyclones on oil and gas operations can be severe with respect to damage to infrastructure as well as threatening personnel safety. The cessation and reconnection of loading of vessels from offshore gas risers or from fixed or floating platforms plus the evacuation and the postcyclone redeployment of personnel from offshore infrastructure is extremely expensive. Costs of specific incidents arising from TC transit through the NWA shelf region have been assessed at between AUD $50 million and AUD $125 million, including damage to offshore infrastructure, vessels, and lost production. The requirement for improving the quality of tropical cyclone forecasting (cyclogenesis, track projection, drift velocity, severity of winds, radius to maximum winds, landfall, etc.) in this region continues given increased investment in the region. This statistical work indicates that this TC basin is likely to be very sensitive to climate change, and NWA is under increasing threat from more severe TCs. Thus, this study serves as a preliminary step for a series of studies aiming at improving TC projection for the NWA region.

Acknowledgments. The authors thank Prof. Michael Richman, School of Meteorology, University of Oklahoma, for several discussions about the theory and application of nonparametric tests of significance. Mr. Stan Stroud from Woodside provided the information on the cost of poorly forecast cyclones on oil and gas industries over northwest Western Australia. In the revision stage, Prof. Mervyn Lynch went out of his way to help in the rewriting of the manuscript.

References

Bender, M. A., T. R. Knutson, R. E. Tuleya, J. J. Sirutis, G. A. Vecchi, S. T. Garner, and I. M. Held, 2010: Modeled impact of anthropogenic warming on the frequency of intense Atlantic hurricanes. *Science*, **327**, 454–458, doi:10.1126/science.1180568.

Bengtsson, L., K. I. Hodges, M. Esch, N. Keenlyside, L. Kornblueh, J.-J. Luo, and T. Yamagata, 2007: How may tropical cyclones change in a warmer climate? *Tellus*, **59A**, 539–561, doi:10.1111/j.1600-0870.2007.00251.x.

Bretherton, C., J. McCaa, and H. Grenier, 2004: A new parameterization for shallow cumulus convection and its applications to marine subtropical cloud-topped boundary layers. Part I: Description and 1D results. *Mon. Wea. Rev.*, **132**, 864–882, doi:10.1175/1520-0493(2004)132<0864:ANPFSC>2.0.CO;2.

Broadbridge, L., and B. N. Hanstrum, 1998: The relationship between tropical cyclones near Western Australia and the Southern Oscillation index. *Aust. Meteor. Mag.*, **47**, 183–189.

Broccoli, A., and S. Manabe, 1990: Can existing climate models be used to study anthropogenic changes in tropical cyclone climate? *Geophys. Res. Lett.*, **17**, 1917–1920, doi:10.1029/GL017i011p01917.

——, and ——, 1992: Reply [to "Comment on 'Can existing climate models be used to study anthropogenic changes in tropical cyclone climate'" by Evans]. *Geophys. Res. Lett.*, **19**, 1525–1526, doi:10.1029/92GL01670.

Burroughs, W., Ed., 2003: *Climate: Into the 21st Century*. Cambridge University Press, 240 pp.

Camargo, S., A. W. Robertson, S. J. Gaffney, P. M. Smyth, and M. Ghil, 2007a: Cluster analysis of typhoon tracks. Part I: General properties. *J. Climate*, **20**, 3635–3653, doi:10.1175/JCLI4188.1.

——, ——, ——, ——, and ——, 2007b: Cluster analysis of typhoon tracks. Part II: Large scale circulation and ENSO. *J. Climate*, **20**, 3654–3676, doi:10.1175/JCLI4203.1.

Chand, S., J. McBride, K. Tory, M. Wheeler, and K. Walsh, 2013: Impact of different ENSO regimes on central South Pacific tropical cyclones. *J. Climate*, **26**, 600–608, doi:10.1175/JCLI-D-12-00114.1.

Done, J. M., C. A. Davis, L. R. Leung, and Y. Kuo, 2005: Understanding the value of high resolution regional climate modeling. *AMS Forum: Living with a Limited Water Supply*, San Diego, CA, Amer. Meteor. Soc., 5.1. [Available online at https://ams.confex.com/ams/Annual2005/techprogram/paper_83186.htm.]

Eagleson, P. S., 1982: Ecological optimality in water-limited natural soil-vegetation systems: 1. Theory and hypothesis. *Water Resour. Res.*, **18**, 325–340, doi:10.1029/WR018i002p00325.

——, and T. Tellers, 1982: Ecological optimality in water-limited natural soil-vegetation systems: 2. Tests and applications. *Water Resour. Res.*, **18**, 341–354, doi:10.1029/WR018i002p00341.

Emanuel, K. A., 2010: Tropical cyclone activity downscaled from NOAA-CIRES reanalysis, 1908–1958. *J. Adv. Model. Earth Syst.*, **2**, doi:10.3894/JAMES.2010.2.1.

Evans, J., and R. Hart, 2003: Objective indicators of the extratropical transition lifecycle of Atlantic tropical cyclones. *Mon. Wea. Rev.*, **131**, 909–925, doi:10.1175/1520-0493(2003)131<0909:OIOTLC>2.0.CO;2.

Goebbert, K., and L. M. Leslie, 2010: Interannual variability of northwest Australian tropical cyclones. *J. Climate*, **23**, 4538–4555, doi:10.1175/2010JCLI3362.1.

Government of Western Australia, 2013: Western Australian mineral and petroleum statistics digest 2012−13. Government of Western Australia Department of Mines and Petroleum Rep., 80 pp. [Available online at http://dmp.wa.gov.au/documents/statistics_release/2012-13_web_acces_Digest.pdf.]

Hall, J. D., A. J. Matthews, and D. J. Karoly, 2001: The modulation of tropical cyclone activity in the Australian region by the Madden–Julian oscillation. *Mon. Wea. Rev.*, **129**, 2970–2982, doi:10.1175/1520-0493(2001)129<2970:TMOTCA>2.0.CO;2.

Hart, R., 2003: A cyclone phase space derived from thermal wind and thermal asymmetry. *Mon. Wea. Rev.*, **131**, 585–616, doi:10.1175/1520-0493(2003)131<0585:ACPSDF>2.0.CO;2.

——, and J. Evans, 2001: A climatology of the extratropical transition of Atlantic tropical cyclones. *J. Climate*, **14**, 546–564, doi:10.1175/1520-0442(2001)014<0546:ACOTET>2.0.CO;2.

Henderson-Sellers, A., and Coauthors, 1998: Tropical cyclone and global climate change: A post-IPCC assessment. *Bull. Amer. Meteor. Soc.*, **79**, 19–38, doi:10.1175/1520-0477(1998)079<0019:TCAGCC>2.0.CO;2.

Holland, G. J., and P. J. Webster, 2007: Heightened tropical cyclone activity in the North Atlantic: Natural variability or climate trend? *Philos. Trans. Roy. Soc.*, **A365**, 2695–2716, doi:10.1098/rsta.2007.2083.

Horn, M., and Coauthors, 2014: Tracking scheme dependence of simulated tropical cyclone response to idealized climate simulations. *J. Climate*, **27**, 9197–9213, doi:10.1175/JCLI-D-14-00200.1.

Hurrell, J. W., T. N. Palmer, and H. Cattle, 2008: CLIVAR: Annual progress report. Report of the Twenty-Ninth Session of the Joint Scientific Committee of World Climate Research Programme (Arcachon, France, 31 March-4 April 2008), WCRP Rep. WMO/TD-No.1439, 1–81.

Kalnay, E., and Coauthors, 1996: The NCEP/NCAR 40-Year Reanalysis Project. *Bull. Amer. Meteor. Soc.*, **77**, 437–472, doi:10.1175/1520-0477(1996)077<0437:TNYRP>2.0.CO;2.

Kendall, M. G., 1970: *Rank Correlation Methods.* 4th ed. Griffin, 202 pp.

Kim, H., J.-H. Kim, C.-H. Ho, and P.-S. Chu, 2011: Pattern classification of typhoon tracks using the fuzzy *c*-means clustering method. *J. Climate*, **24**, 488–507, doi:10.1175/2010JCLI3751.1.

Kistler, R., and Coauthors, 2001: The NCEP–NCAR 50-Year Reanalysis: Monthly means CD-ROM and documentation. *Bull. Amer. Meteor. Soc.*, **82**, 247–267, doi:10.1175/1520-0477(2001)082<0247:TNNYRM>2.3.CO;2.

Knutson, T. R., and Coauthors, 2010: Tropical cyclones and climate change. *Nat. Geosci.*, **3**, 157–163, doi:10.1038/ngeo779.

Kossin, J., K. Knapp, D. Vimont, R. Murnane, and B. Harper, 2007: A globally consistent reanalysis of hurricane variability and trends. *Geophys. Res. Lett.*, **34**, L04815, doi:10.1029/2006GL028836.

Kruk, M. C., K. R. Knapp, D. H. Levinson, and J. Kossin, 2010: A technique for combining global tropical cyclone best track data. *J. Atmos. Oceanic Technol.*, **27**, 680–692, doi:10.1175/2009JTECHA1267.1.

Lavender, S. L., and K. J. E. Walsh, 2011: Dynamically downscaled simulations of Australian region tropical cyclones in current and future climates. *Geophys. Res. Lett.*, **38**, L10705, doi:10.1029/2011GL047499.

Mann, H., 1945: Nonparametric tests against trend. *Econometrica*, **13**, 245–259, doi:10.2307/1907187.

McDonald, R., D. Bleaken, D. Creswell, and C. Senior, 2005: Tropical storms: Representation and diagnosis in climate models and the impacts of climate change. *Climate Dyn.*, **25**, 19–36, doi:10.1007/s00382-004-0491-0.

McLeod, A., K. Hipel, and B. Bodo, 1991: Trend analysis methodology for water quality time series. *Environmetrics*, **2**, 169–200, doi:10.1002/env.3770020205.

Murakami, H., and M. Sugi, 2010: Effect of model resolution on tropical cyclone climate projections. *SOLA*, **6**, 73–76, doi:10.2151/sola.2010-019.

——, and B. Wang, 2010: Future change of North Atlantic tropical tracks. *J. Climate*, **23**, 2699–2721, doi:10.1175/2010JCLI3338.1.

——, ——, and A. Kitoh, 2011: Future change of western North Pacific typhoons: Projections by a 20-km-mesh global atmospheric model. *J. Climate*, **24**, 1154–1169, doi:10.1175/2010JCLI3723.1.

Oouchi, K., J. Yoshimura, H. Yoshimura, R. Mizuta, S. Kusunoki, and A. Noda, 2006: Tropical cyclone climatology in a global warming climate as simulated in a 20-km-mesh global atmospheric model: Frequency and wind intensity analysis. *J. Meteor. Soc. Japan*, **84**, 259–276, doi:10.2151/jmsj.84.259.

Putman, W., and S.-J. Lin, 2007: Finite-volume transport on various cubed-sphere grids. *J. Comput. Phys.*, **227**, 55–78, doi:10.1016/j.jcp.2007.07.022.

Ren, D., M. Lynch, L. M. Leslie, and J. Lemarshall, 2014: Sensitivity of tropical cyclone tracks and intensity to ocean surface temperature: Four cases in four different basins. *Tellus*, **66A**, 24212, doi:10.3402/tellusa.v66.24212.

Rotunno, R., Y. Chen, W. Wang, C. Davis, J. Dudhia, and G. Holland, 2009: Large-eddy simulation of an idealized tropical cyclone. *Bull. Amer. Meteor. Soc.*, **90**, 1783–1788, doi:10.1175/2009BAMS2884.1.

Scott, D. W., 1992: *Multivariate Density Estimation: Theory, Practice, and Visualization.* Wiley, 317 pp.

Stowasser, M., Y. Wang, and K. Hamilton, 2007: Tropical cyclone changes in the western North Pacific in a global warming scenario. *J. Climate*, **20**, 2378–2396, doi:10.1175/JCLI4126.1.

Walsh, K., 2004: Tropical cyclones and climate change: Unresolved issues. *Climate Res.*, **27**, 77–83, doi:10.3354/cr027077.

——, M. Fiorino, C. Landsea, and K. McInnes, 2007: Objectively determined resolution-dependent threshold criteria for the detection of tropical cyclones in climate models and reanalyses. *J. Climate*, **20**, 2307–2314, doi:10.1175/JCLI4074.1.

Wang, Y., Y. Wang, and H. Fudeyasu, 2009: The role of Typhoon Songda (2004) in producing distantly located heavy rainfall in Japan. *Mon. Wea. Rev.*, **137**, 3699–3716, doi:10.1175/2009MWR2933.1.

Wu, L., and B. Wang, 2004: Assessing impact of global warming on tropical cyclone tracks. *J. Climate*, **17**, 1686–1698, doi:10.1175/1520-0442(2004)017<1686:AIOGWO>2.0.CO;2.

Yokio, S., and Y. Takayabu, 2009: Multi-model projection of global warming impact on tropical cyclone frequency over the western North Pacific. *J. Meteor. Soc. Japan*, **87**, 525–538, doi:10.2151/jmsj.87.525.

Zhao, M., and I. M. Held, 2010: An analysis of the effect of global warming on the intensity of Atlantic hurricanes using a GCM with statistical refinement. *J. Climate*, **23**, 6382–6393, doi:10.1175/2010JCLI3837.1.

——, ——, S.-J. Lin, and G. A. Vecchi, 2009: Simulations of global hurricane climatology, interannual variability, and response to global warming using a 50-km resolution GCM. *J. Climate*, **22**, 6653–6678, doi:10.1175/2009JCLI3049.1.

Earth Interactions is published jointly by the American Meteorological Society, the American Geophysical Union, and the Association of American Geographers. Permission to use figures, tables, and *brief* excerpts from this journal in scientific and educational works is hereby granted provided that the source is acknowledged. Any use of material in this journal that is determined to be ''fair use'' under Section 107 or that satisfies the conditions specified in Section 108 of the U.S. Copyright Law (17 USC, as revised by P.IL. 94-553) does not require the publishers' permission. For permission for any other from of copying, contact one of the copublishing societies.